Properties of nanostructured ZnO thin films synthesized using a modified aqueous chemical growth method

To cite this article before publication: Oliver O Apeh *et al* 2018 *Mater. Res. Express* in press https://doi.org/10.1088/2053-1591/aadcd6

Properties of Nanostructured ZnO thin films Synthesized Using a Modified Aqueous Chemical Growth Method

Oliver O. Apeh[a,b], Ugochi K. Chime[a], Solomon Agbo[c], Sabastine Ezugwu[d.], Raymond Taziwa[b], Edison Meyer[b], Pavol Sutta[e], Malik Maaza[f,g], Fabian I. Ezema[a,f,g,h*]

[a]Department of Physics and Astronomy, University of Nigeria Nsukka Nigeria
[b]Fort Hare Institute of Technology (FHIT), 1 Fort Hare Drive, 3rd Floor Chemistry Building, University of Fort Hare, Alice 5700, South Africa.
[c]Alexander von Humboldt Research fellow, Institute of Energy and Climate Research (IEK-5), Julich, Germany.
[d]Department of Physics and Astronomy, University of Western Ontario, Canada
[e]New Technologies Research Centre, University of West Bohemia,Univerzitni 8, 306 14 Pilsen, Czech Republic
[f]Nanosciences African Network (NANOAFNET), iThemba LABS-National Research
[g]UNESCO-UNISA Africa Chair in Nanosciences/Nanotechnology, College of Graduate Studies, University of South Africa (UNISA), Muckleneuk ridge, P.O. Box 392, Pretoria, South Africa
[h]Department of Physics, Faculty of Natural and Applied Sciences, Coal City University, Enugu, Nigeria

Abstract

Research and development of nano-sized Zinc Oxide (ZnO) has recently received great attention due to its remarkable properties such as large exciton binding energy of 60 meV, extraordinary photosensitivity, nontoxic nature, wide bandgap and the fact that it is a low cost material with many technological applications. The inherent necessity for stoichiometric ZnO nanostructures suggest that a deposition method where the film stoichiometry is controlled by a chemical reaction is un-avoidable. Moreover, it is extremely important, when developing new methods for deposition of ZnO nanostructures to keep the deposition system as simple as possible, maximize throughput, and keep costs at a minimum. Modified aqueous chemical growth method offer such an opportunity. In this work, ZnO nano-petals on microscope glass substrates have been prepared by using a modified aqueous chemical growth method. On the other hand, before utilization of the fabricated ZnO nanostructures by any technique for any technological applications, it is essential to investigate morphological, optical, electrical and structural properties. In this work morphological, optical, electrical and structural properties with respect to change in deposition time have been cross examined using FESEM, UV-Vis spectroscopy, I-V properties by Keithley system and XRD respectively. SEM micrographs have revealed very little changes in the shape, orientations and distribution of ZnO nano-petals formed with change in deposition times. SEM micrographs have also revealed the growth pattern for the prepared ZnO nano-petals which proceeds via a nucleation, and coalescence of ZnO nuclei. XRD analysis have revealed that the synthesized ZnO nano-petals have a hexagonal Wurtzite ZnO structure with peaks at 2θ positions 31.7°, 34.4°, 36.2°, 47.4°, 56.5°and 62.7° belonging to the (100), (002), (101), (102), (110) and (103) planes respectively. UV-Vis spectroscopy has in the same way shown that the synthesized ZnO nano-petals have energy band gaps ranging from 3.46 eV to 3.65 eV. I-V measurements have disclosed that the ZnO nano-petals are conductive. Film resistivity values obtained from the I-V curves showed an exponential increase in resistivity with increased film thickness. Our method of preparation of ZnO nano-petals via a chemical assisted route can serve as benchmark for controlled synthesis of ZnO nanostructures for various technological applications.

*Author to whom corresponding should be addressed (F.I. Ezema):

E-mail address: fabian.ezema@unn.edu.ng,
+2348036239214
Key words: Aqueous chemical growth; ZnO; Deposition time; nano petals.

1. Introduction

ZnO is a group II–VI semiconductor material with characteristic optical, transport and piezoelectric properties [1]. It has a wurtzite structure and a wide band-gap of about 3.4 eV, which makes it suitable for optoelectronic applications at short wavelengths [2–4]. It also has a high exciton binding energy of 60 mV at room temperature which has been reported to yield good excitonic emission at ultraviolet spectrum in disordered nanoparticles [5]. Because of its high optical transparency in the visible and excellent electrical properties, especially when doped by aluminium [3], thin films of ZnO and ZnO-based materials have received enormous research attention in applications ranging from electrodes for solar cells and optoelectronic devices; to sensors and piezoelectric transducers, among other applications [1-10]. They are widely studied as alternative transparent conducting oxide (TCO) to mitigate the high cost of indium tin oxide (ITO) caused by the scarcity of indium. These studies have also produced large spectrum of ZnO nano-assemblies with different morphologies, including nanowires [6], nanorods [7], nanopillars [8], nanorings [9], nanospikes [10], nanoflakes [11], nanoflowers [12], and nanopencils [13].

With the progress made so far on arrays of different ZnO nano-assemblies that can be fabricated, the necessity to utilize high quality ZnO nanostructures in devices suggest that a deposition method where the film quality is controlled by a chemical reaction is un-avoidable. Moreover, it is an inherent requirement, when developing new methods for deposition of ZnO nanostructures to keep the deposition system as simple as possible, maximize throughput and keep costs at a minimum. To date, these requirements have not been satisfactorily met as most reported quality ZnO nanostructures requires high cost and complex deposition systems/methods such as RF magnetron sputtering, photo-atomic layer deposition, chemical vapour deposition [15], ultrasonic pyrolysis [16] and thermal evaporation [14-19]. Indeed, aqueous chemical growth method offers an alternative platform and the prospect of a deposition process at low cost and moderate temperatures. The method has the advantage of non-toxicity, reproducibility and suitability for deposition on a variety of substrates [20-21]. More intriguing is the prospect of good control of sample morphology despite the fact that controlling thin film morphology of inorganic materials is a demanding experimental challenge [22]. In the case of chemical growth method, the morphology of ZnO thin films can be tuned by utilizing such experimental factors as concentration [23], pH of

precursor [24], type of substrate used [25], deposition temperature and deposition time [26, 27].

Herein, we investigate the effects of deposition time on the properties of ZnO nanostructural thin films fabricated using a modified aqueous chemical growth method. A decisive advantage of varying the deposition time is that it directly controls the film thickness, and consequently the properties of the samples. For instance, crystallite size and orientation can be tuned on the basis of the films thickness and by extension the grain boundary and porosity of such thin films. Our deposition method utilizes ZnO seed layer fabricated at an optimized time of 10 seconds in a dilute solution of zinc acetate to create nuclei on which ZnO crystals can grow in solution. We show that our method preserves the flower-like structure and the orientations of the needle-like crystals emanating from a single 'flower' of ZnO nanostructured thin films fabricated at four different deposition times of 15, 20, 25 and 30 minutes respectively. A comprehensive results and discussion on the morphological, optical, electrical and structural properties of these samples will be presented.

2. Experimental details

Reproducible ZnO nanostructures have been prepared via a two stage process: step (I) through a wet chemical process that involves the formation of thin layer of ZnO nano-seeds on the surface of a microscope glass slide and second step (II) for the growth of ordered ZnO nanostructures by refluxing the ZnO nano-seeds at different times. In a typical synthesis route, non-conductive microscope glass slides were ultrasonically cleaned in acetone and methanol and subsequently dried in air prior to use. As shown in Fig.1, 0.3 M Zinc acetate ($Zn(CH_3COO)_2.2H_2O$) precursor solution was prepared by dissolving 50 ml of ethanol in 'beaker A'. 1.097 g of diethanolamine ($HN(CH_2CH_2OH)_2$, DEA) was dissolved in 100 ml of ethanol in 'beaker B'. The content of the two beakers were then poured simultaneously to another beaker and ultrasonically mixed prior to thin film deposition. To form ZnO seed layer, glass substrates were dipped in the precursor solutions for 10 seconds and allowed to dry in air at room temperature for 24 hrs. The coated substrates were annealed at 350 °C for 5 minutes to form uniform seed layer on the glass slides.

Figure 1 also presents the refluxing apparatus used in preparation of ZnO nanostructures. A sample holder was fabricated out of glass block for accurate and reproducible positioning of the substrates during all the depositions. One end of the holder is a cylindrical block that fits and seal the neck of the conical flask, whereas the opposite end of the holder is rectangular in shape, engineered at the centre to allow 5 mm wide glass to be

fastened and held in position during thin film depositions. The precursor was maintained at a predetermined temperature using the refluxing set up shown here in Figure 1. In this way, the thin film depositions were uniquely maintained at predetermined conditions.

To deposit nanostructured ZnO thin films, the substrate/ZnO seed layer was inserted in the conical flask containing 200 ml solution of 0.05 M zinc acetate and 0.05 M hexamethylenetetramine (HMTA), with the heating mantle maintained at a steady temperature of 85 ^{o}C. Four samples of a hierarchical based ZnO thin films were allowed to grow in a sequence of nucleation, coalescence and cluster growth for different time durations of 15, 20, 25 and 30 minutes respectively. This method of deposition of zinc oxide thin film in an aqueous solution is based on controlled precipitation on the substrate via condensation reaction of zinc ion. The as-grown films were rinsed in distilled water to remove the loose and residual part of the deposited material and subsequently allowed to dry in air at room temperature.

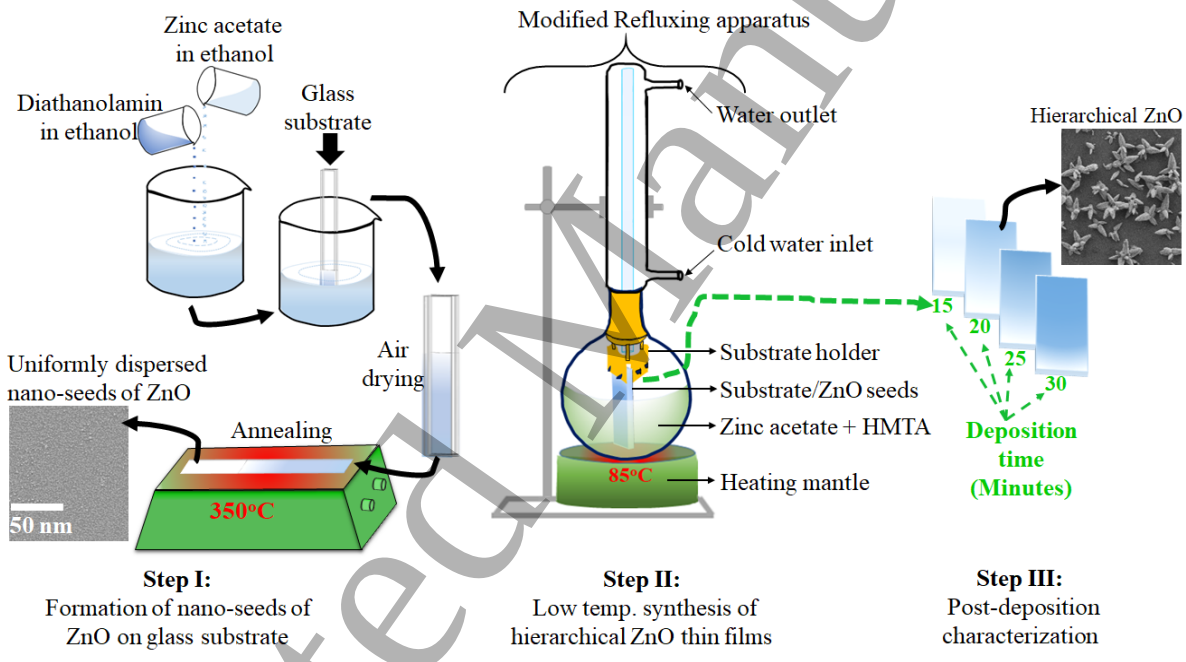

Figure 1: Schematic demonstration of synthesis steps of ZnO thin films studied in this work.

At an optimized short dip time of 10 seconds in a dilute solution of zinc acetate and subsequent high temperature thermal annealing for 5 minutes, nano-sized seed layer of ZnO is grown on a microscope glass slide. In the second step, the refluxing apparatus equipped with home-made substrate holder is used to grow hierarchical, flower-like structured ZnO at four different deposition times of 15, 20, 25 and 30 minutes. The substrate holder ensures that the substrate/ZnO seeds are retained in the same upright position throughout the deposition time.

The morphology of the ZnO nanostructures was cross examined using a LEO (Zeiss) 1540 field scanning electron microscope FESEM. Witec Alpha300S atomic force microscopy was used to study the thickness of our ZnO nanostructural thin films. To obtain the thickness, artificial steps were created on the sample surface with soft probes that were known not to scratch the substrate. A 10 μm by 10 μm AFM scan was subsequently carried out on the sample-substrate interface. The line profile of the step at the interface was then used to determine the thickness of the samples. The crystalline structure and identification of phases were studied using XRD technique. The optical properties were investigated using CARY 5E UV-Vis-NIR spectrophotometer. The vibrational modes were observed using the Raman Spectroscopy technique.

The current-voltage (I-V) characteristics of ZnO thin films were obtained using a Keithley 2400 source meter operated in the range of ±3 V. The set-up for measuring the I-V characteristics of the films at different thicknesses is shown in Fig. 2. Aluminum contacts of length L, in which two adjacent stripes are separated by a gap w, were used as contact for applied voltage, V_a. In this configuration, the in-plane surface conductivity is expected to play a dominate role over the bulk electrical conduction, which is generally observed in sandwich configuration.

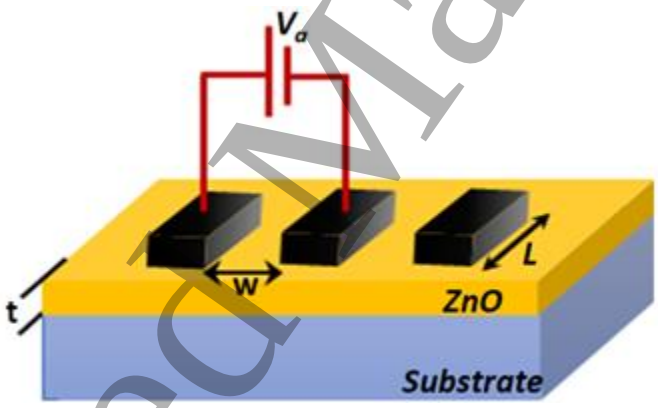

Figure 2: The configuration for measuring the I-V characteristics of ZnO thin films of different thicknesses in which V_a is the applied voltage to drive current through the ZnO sample of thickness, t. The configuration includes thermally evaporated Al contact of uniform length, L and separation, w.

3. Results and discussion

3.1. SEM analysis

SEM studies were conducted to examine the effect of deposition time on the surface morphology of ZnO nanostructures prepared by a modified aqueous chemical growth method. The SEM images presented in Fig. 3 show sparsely distributed flower-like structures

with bud-like nanopetals that grow from the centre of each 'nanoflowers'. These ZnO nanoflowers are formed even at 15 min. deposition time and grow in size and length with time, as expected. The length of the nanopetal estimated from the SEM micrograms shows a growth rate of 4 nm/min. from the centre of the nanoflower. Their values are 20 nm, 30 nm, 45 nm and 80 nm at deposition time of 15, 20, 25 and 30 minutes respectively. While the size and density of the ZnO nanoflower/nanocluster grows as the deposition time increases, the shape, orientations and distribution of the nanostructures remain essentially the same even at highest deposition time of 30 minutes. The homogeneity in shape and consistent nanostructure of the samples even at double of the initial deposition time can be attributed to the presence of the seed layer which acts as the building block for the growth of these nanostructures. The significant of maintaining a consistent deposition conditions, including temperature of the aqueous solution, substrate position and pH of the solution bath cannot be ruled out. Changing these deposition conditions can potentially alter the morphology of chemically fabricated nanostructured thin films [28–30].

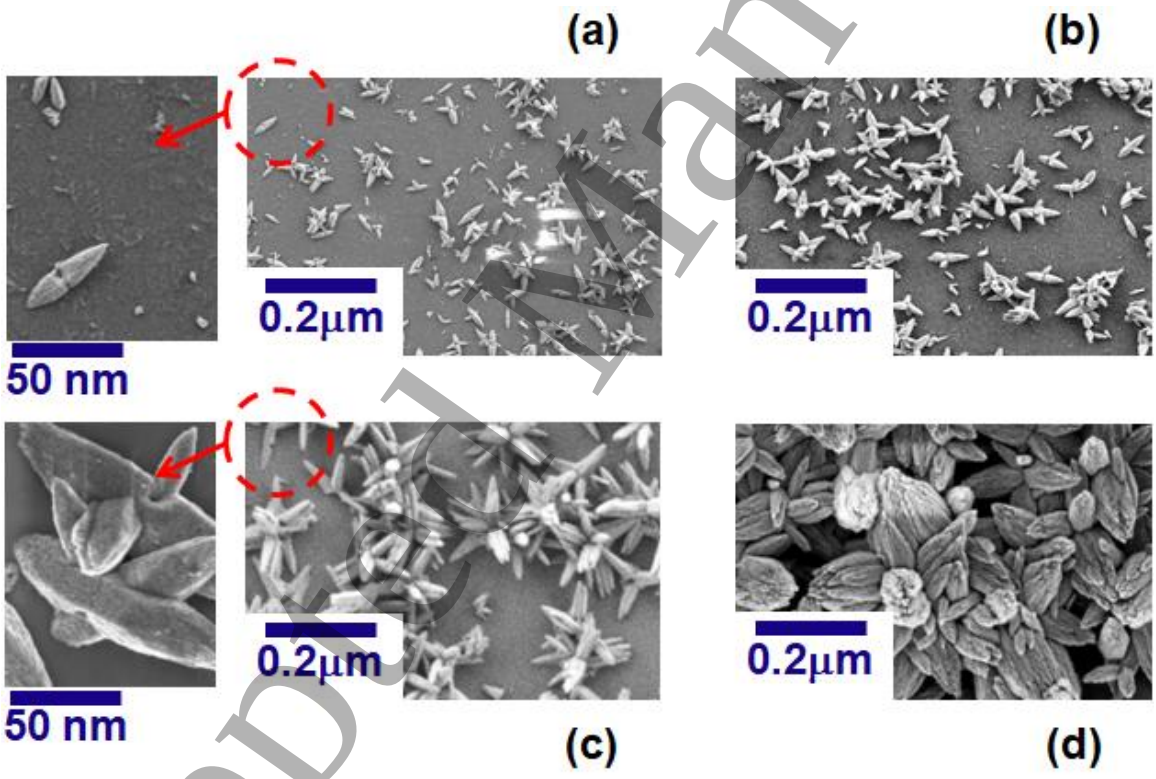

Figure 3: FESEM images of nanosctructured ZnO thin films deposited at different refluxing times of (a) 15 mins, (b) 20 mins, (c) 25 mins and (d) 30 mins The images were acquired at 12.5 K. Included on the left is 50 K magnified images of (a) and (c) for clarity. Irrespective of dip time, the images indicate similar growth pattern of nucleation, coalescence and subsequent growth of individual clusters.

The magnified images of Fig. 3(a) and 3(b) have revealed the ideal growth pattern of these ZnO nanoflowers prepared by our method. The growth pattern proceeds via nucleation and growth from existing ZnO nanoseeds. ZnO seeds serve as the initial nuclei on which impinging Zn and O/OH ions nucleate in controlled manner via condensation reactions reminiscent of assisted chemical reactions [23,28,31–32]. The actual nucleation and growth of the sample from these precipitates follows exactly the Volmer-Weber growth mode [33]. The growth of the initial island of ZnO is favoured because the atoms and ions in the condensation share stronger bonds with each other than with the substrate. The fabrication of ZnO island seed on glass substrate were activated by high temperature annealing at 350 ^{o}C. Once the seed layer is fabricated, they become the rallying point for nucleation and growth by Volmer-Weber growth mode as depicted in Fig. 4. The evolution of ZnO nanoflower begins as soon as ZnO precipitates are formed under refluxing conditions described earlier in Fig. 1. The precipitates stick and nucleate on the ZnO seed and grow in different directions, away from the central seed to form flower-like structures. Coalesces of latter nuclei can also occur and is primarily responsible for increase in density of the nanoflowers and surface area coverage observed in the SEM image after deposition at 25 mins. This can also lead to rapid increase of thickness of the sample as we show in the following section.

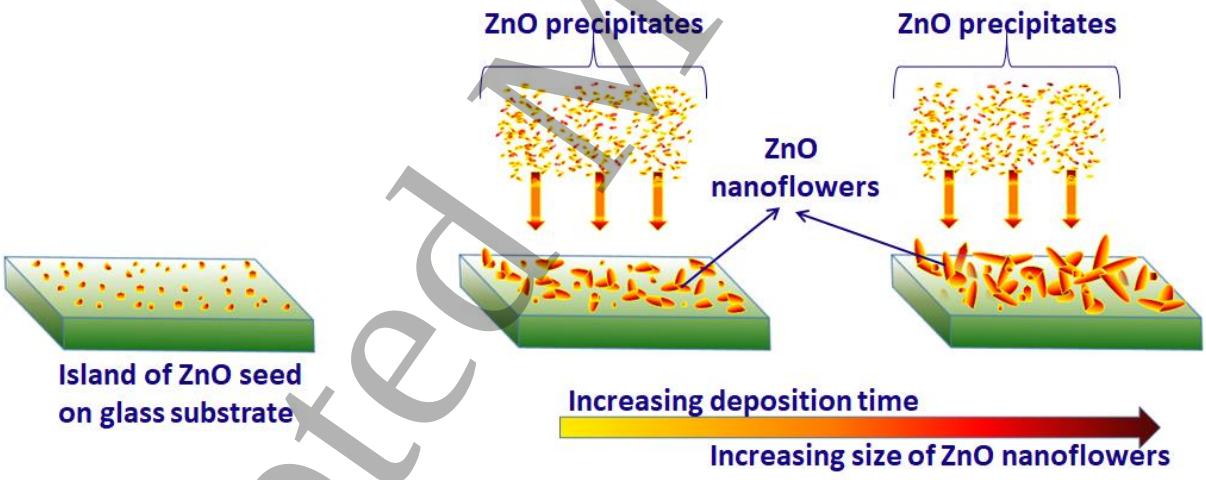

Figure 4: Heterogeneous growth of ZnO on glass substrate described by Volmer-Weber growth mode.

The fact that impinging atoms tend to nucleate on existing ZnO seeds more than the glass substrate can be a consequence of the interfacial free energy and possible lattice mismatch between the substrate and the condensation species. The Young-Dupre equations is a useful tool to describe accurately the relationship between the surface energies in most heterogeneous thin films growth [34,35]:

$$\gamma_{SV} = \gamma_{FL} + \gamma_{FV} \cdot Cos(\alpha) \quad (1)$$

In this equation, γ is the surface energy, SV is substrate-vapour, FL is film-liquid and FV is the film-vapour, and α is the contact angle. These surface energies play significant role in determining how ZnO precipitates grow on the substrate surface. When the substrate surface energy is sufficiently high, the substrate tends to provide a good adhesive 'wet out' on which rapid and uniform surface coverage of the growing species can be achieved. If, on the other hand, γ_{FL} is comparatively higher, then ZnO seeds serve as the building block for the formation of final product. Hence, nucleation and island/cluster growth is favoured at the opposite of planar growth when the film-liquid interfacial energy, γ_{FL} and film-vapour surface energy, γ_{FV} are high enough to satisfy the following inequality:

$$\gamma_{SV} < \gamma_{FS} + \gamma_{FV} \quad (2)$$

It is well known [36–41] that the contact angle of reported ZnO nanostructures are always greater than zero, which satisfies eq. (2) above. Although wettability study was not carried out in the present work, visual inspection of SEM images in Fig. 3 clearly shows that the deposited ZnO nanostructures are inclined to the substrate in conformity to eqs. (1) and (2). The SEM images also indicate that the unique advantage of the modified aqueous chemical growth method adopted in the present work is that the morphological evolution at different deposition time preserves the structure and orientation of the deposited ZnO samples. This can serve as a benchmark for synthesis of a variety of nanostructured thin films and study of their properties that are generally morphology dependent.

3.2 Atomic Force Microscopy (AFM)

The AFM morphological images, roughness and the thickness were determined on each sample using a Witec Alpha300S atomic force microscope (AFM) operating in tapping mode. Fig 5(a-d) shows the 3-dimensional AFM images obtained at different deposition times. The results indicate that variation in deposition time had a significant effect on the density of the ZnO nanostructures, in conformity with SEM micrograph. The z-scale of the AFM topographic images shows an out-of-plane growth favoured at higher deposition times. The estimated length of the ZnO nanoclusters from AFM images are 89 nm, 112 nm, 186 nm and 258 nm for the samples deposited at 15, 20, 25 and 30 minutes, respectively. These values are for the entire length of nanoclusters, which are different from the values of single ZnO nanopetals obtained previously from the SEM micrographs.

Fig. 5(e) shows that the thickness of the ZnO nanoclusters increases as the depositions time in conformity to the observed z-scale values. The result also shows rapid increase in the

thickness after 25 min of ZnO deposition. The root mean square (RMS) roughness is highest in the sample deposited after 20 min. and decreases to a minimum after 30 min. deposition time (Fig. 5f). From the AFM and SEM images, it can be inferred that 20 min. represents the optimum depositions time for complete formation of ZnO nanoflower from existing seed layers. Above the 20 min. mark, the nanoclusters grow very rapidly both in size and height from the impinging Zn^{2+} and OH^{-} species in solution. This is responsible for the rapid increase in the cluster thickness observed in Fig. 5e and decrease in the sample roughness shown in panel (f).

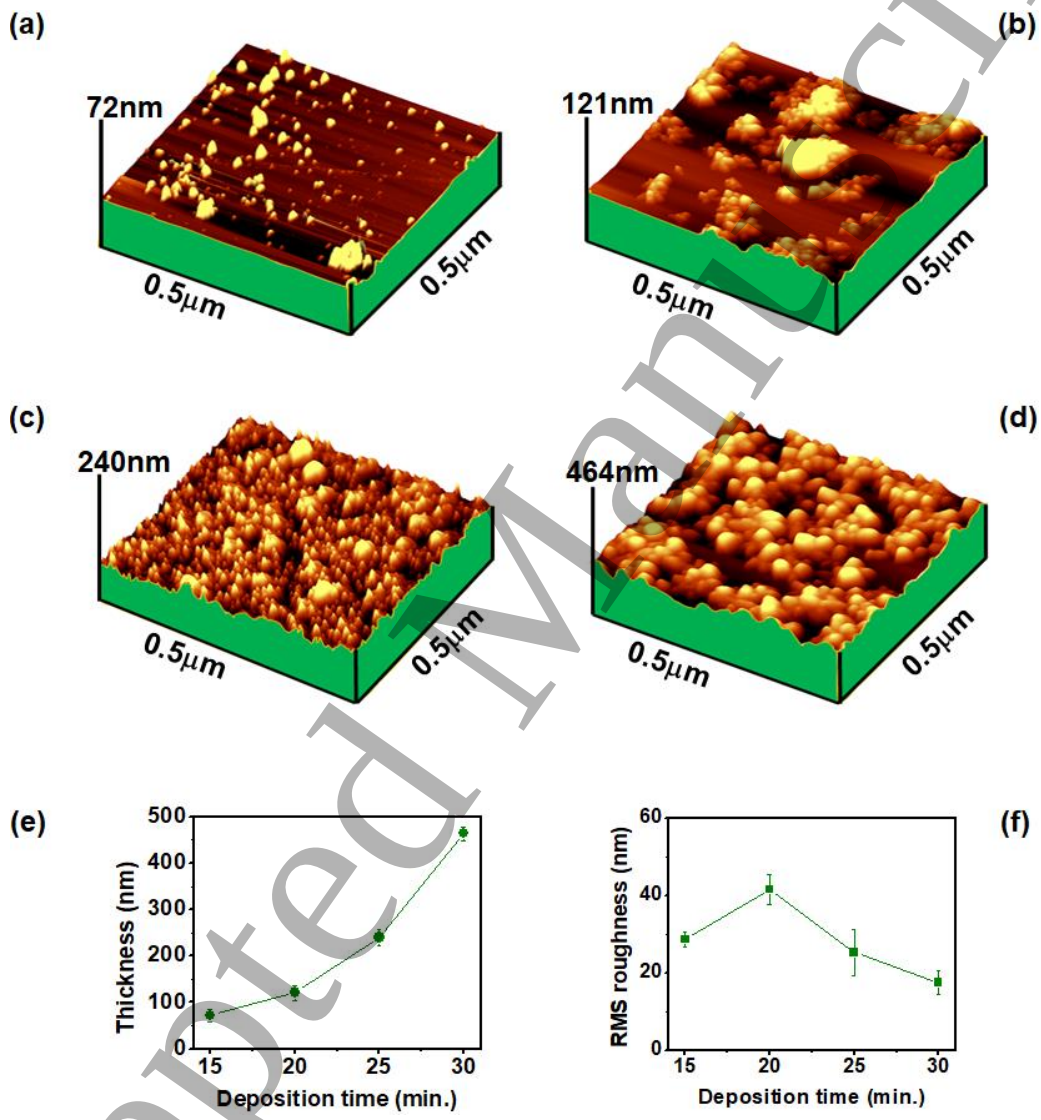

Figure 5: Three dimensional AFM topographic images of ZnO thin films deposited at (a) 15 mins. (b) 20 mins. (c) 25 mins. and (d) 30 mins. (e) Thickness of ZnO thin films versus the deposition time and (f) Variation of the RMS roughness with the deposition time.

3.3 X-ray Diffraction (XRD)

Figure 6 presents the XRD diffractograms of the ZnO nano-petals prepared by a modified aqueous chemical growth method. Figure 6, has revealed diffraction peaks at 31.7°, 34.4°, 36.2°, 47.4°, 56.5°and 62.7° respectively belonging to the (100), (002), (101), (102), (110) and (103) planes with (002) being the most prominent. All of these peaks exhibit the characteristic peaks of hexagonal Wurtzite structure as evidenced by JCPDS data to be zincite 01-070-2551 phase). The intensity along the (002) plane increased as the deposition time increased which indicates that large amount of bulk of crystallites are oriented along (002) plane.

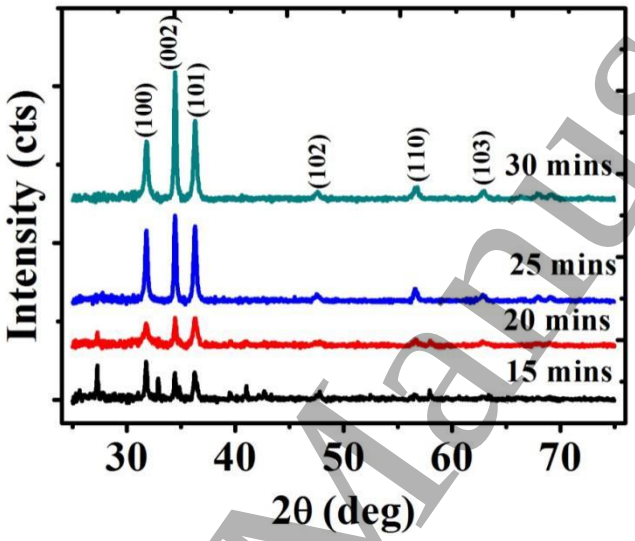

Figure 6: XRD patterns of nanostructured ZnO thin films deposited at different time intervals of 15, 20, 25 and 30 minutes. The diffraction peaks decrease in intensity as the deposition time.

Table 1 and Table 2 show the values of different parameters calculated from the XRD diffraction plots. The average crystallite sizes (D) were obtained from the diffraction line broadening using Scherrer's formula [42].

$$D = \frac{0.9\lambda}{\beta Cos\theta}, \quad (3)$$

where D is the grain diameter, β is the full width at half maximum (FWHM) (in radians), λ is the wavelength of the monochromatic light used (1.54178Å) and θ is the Bragg's angle. The average sizes of the ZnO nanocrystals obtained increased with an increase in film thickness. The lattice strain, ε, which is as a result of distortion and inhomogeneity was calculated using the equation (2) [43].

$$\varepsilon = \beta / 4\tan\theta \quad (4)$$

The interplanar distance at the 002 plane, d, which is the vertical spacing between parallel atomic planes in a crystal was calculated using equation (5) [44]. An increase in the film thickness from 72 nm to 121 nm showed a minute change in interplanar distance from 0.2602 nm to 0.2600 nm. Thereafter, the interplanar distance remains constant.

$$d = \lambda / 2\sin\theta \quad (5)$$

The lattice constants *a* and *c* were calculated using equations (6) and (7) respectively [45].

$$a = \lambda / \sqrt{3}\sin\theta \quad (6)$$

$$c = \lambda / \sin\theta \quad (7)$$

The strain towards the *a*-axis (ε_a) and *c*-axis (ε_c) were calculated using equations (8) and (9) respectively [46].

$$\varepsilon_a = \frac{(a - a_{bulk})}{a_{bulk}} \quad (8)$$

$$\varepsilon_c = \frac{(c - c_{bulk})}{c_{bulk}} \quad (9)$$

Where a_{bulk} (0.324 nm) and c_{bulk} (0.52 nm) are the lattice constants of unstrained ZnO. The low values of ε_a and ε_c in Table 1, indicate that there is little strain on the deposited ZnO films compared to that of bulk unstrained ZnO films.

Table 1: Lattice parameters of ZnO at different deposition times

Time, t (mins)	Thickness (nm)	FWHM	D (nm)	ε	d (nm)	a (nm)	c (nm)	ε_a	ε_c
15	72	0.2093	41.59	0.002591	0.2602	0.3248	0.52042	0.002813	0.0008022
20	121	0.2073	42.10	0.003046	0.2600	0.3251	0.52004	0.003072	0.0000698
25	240	0.2068	42.20	0.003475	0.2600	0.3246	0.52004	0.002554	0.0000698
30	464	0.1628	53.45	0.003997	0.2600	0.3243	0.52004	0.002296	0.0000698

The Zn-O bond length was calculated using equations (10) and (11) [47]

$$L = \sqrt{\left(\frac{a^2}{3} + \left(\frac{1}{2} - u\right)^2 c^2\right)} \quad (10)$$

$$u = \frac{a^2}{3c^2} + 0.25 \quad (11)$$

Where *u* is a positional parameter for Wurtzite structures.

The values of the bond length ranged from 0.197420 nm to 0.197743 nm which is remarkably close to the ideal value for bulk zinc (1.9767 nm) [48]. This also indicates very

little compressive strain of the deposited films. The positional parameter values were slightly greater than the ideal Wurtzite phase of hexagonal ZnO which is 0.375 [46].

The bond angles α and β were obtained using equation (12) and (13) respectively [46].

$$\alpha = \frac{\pi}{2} + \cos^{-1}\left[\left(\sqrt{1+3\left(\frac{c}{a}\right)^2\left(\frac{1}{2}-u\right)^2}\right)^{-1}\right] \quad (12)$$

$$\beta = 2\sin^{-1}\left[\left(\sqrt{\frac{4}{3}+4\left(\frac{c}{a}\right)^2\left(\frac{1}{2}-u\right)^2}\right)^{-1}\right] \quad (13)$$

The calculated bond angles α ranging from 108.354^0 to 108.484^0 is only slightly lower than that of the ideal value while β ranging from 110.423° to 110.548° is only slightly greater that the ideal bond angle value given as 109.47°.

Table 2: Positional parameter, bond length, bond angles α and β, *c/a* ratio

Time, t (mins)	u	L (nm)	α (deg)	β (deg)	*c/a*
15	0.379850	0.197681	108.437	110.468	1.6022
20	0.380248	0.197743	108.354	110.548	1.5998
25	0.379833	0.197527	108.441	110.464	1.6023
30	0.379626	0.197420	108.484	110.423	1.6035

3.4 Optical Properties

Figure 7 (a-d) shows the transmittance, absorbance and reflectance curves respectively for ZnO nanoflowers obtained at different deposition times. An increase in deposition time showed a decrease in the transmittance in shown 7(a). A sharp increase in the transmittance is noticed at the visible light region and is found to be consistent with ZnO thin films obtained in ref. 28. The average transmittance in the visible spectrum was obtained to be 69%, 61%, 47% and 41% for 15, 20, 25 and 30 mins deposition times respectively. The absorbance, *A* (panel b) and reflectance, *R* (panel c) data were obtained using equations (14) and (15) respectively.

$$A = \log\frac{1}{T} \quad (14)$$

$$R = 1-(T+A) \quad (15)$$

where T is the transmittance. The absorbance curve in 7(b) shows a sharp decrease in the visible light spectrum with the lowest absorption being from the sample obtained at 15 mins deposition time. The reflectance curve on the other hand showed a fluctuation between 300 and 400 nm wavelengths before maintaining a near constant value at the visible light region. This is also consistent with ZnO reflectance curve reported in the literature [49].

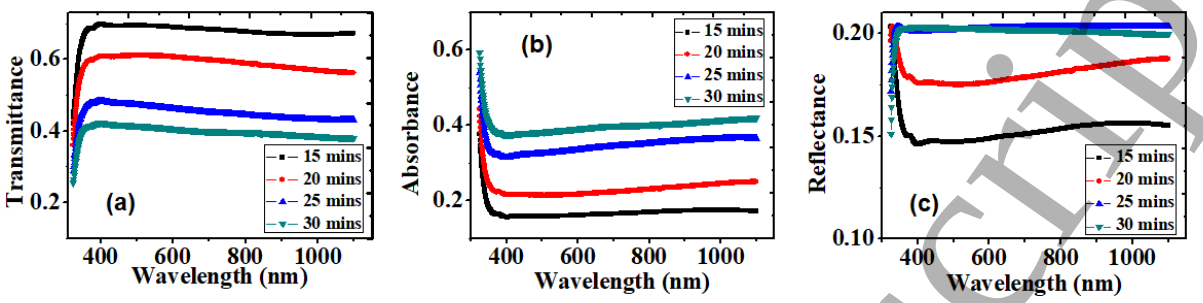

Figure 7: Normal incidence (a) transmittance (b) absorbance and (c) reflectance spectra of nanostructured ZnO thin films at different deposition times.

The absorption coefficient was obtained using equation (16) [50]:

$$\alpha = \frac{1}{d}\ln\left(\frac{(1-R)^2}{T}\right) \tag{16}$$

where α is the absorption coefficient and d is the film thickness. The absorption and extinction coefficient curves are shown in figure 8(a-b). A sharp decrease occurred in the absorption coefficient around the absorption edge. The average absorption coefficient was calculated to range from 6.66 – 12.88 x 10^5 cm^{-1} in the visible light spectrum. The trend of the extinction coefficient k with respect to the wavelength shown in Fig. 8(b) agrees with the behaviour of the absorption coefficient since α is the main factor in the calculation of k.

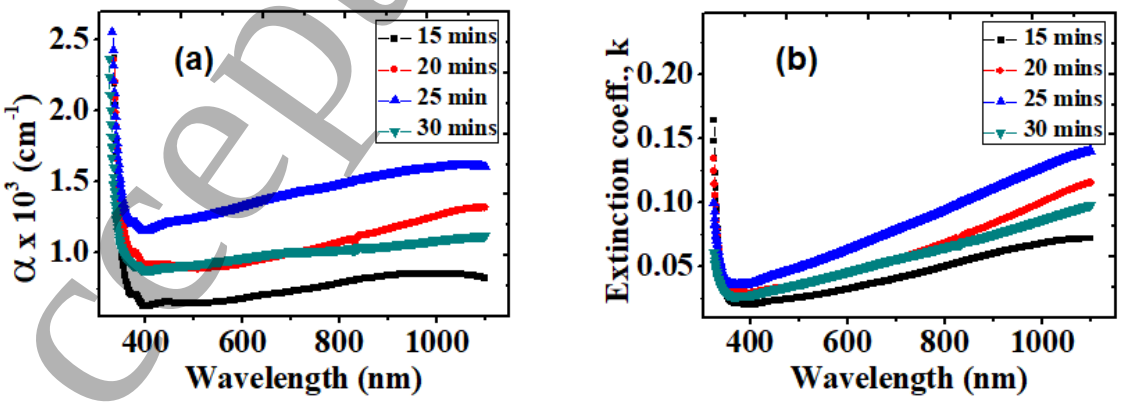

Figure 8: (a) Absorption coefficient and (b) extinction coefficient of nanostructured ZnO thin films at different deposition times.

The bandgap curves are shown in Figure 9(a-d). The bandgap values obtained ranged from 3.46 eV to 3.65eV. The result shows that the band gap energy decreased with the time of deposition from 15 to 25 mins. and reverts to a high value at 30 mins. While the cause of this swift shift of trend is not certain, it could be as a result of the relatively higher value of lattice strain observed in the sample deposited at 30 minutes. Although the lattice spacing reported previously on Table 1 remained constant, distortion due to increased strain can produce defect sites with trapped carriers in the grain boundary which can increase the optical band gap.

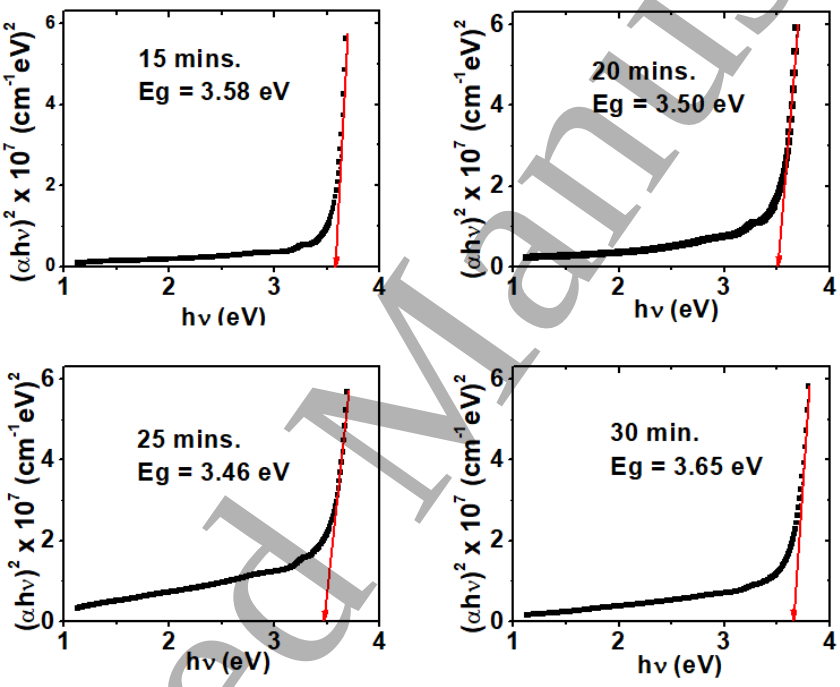

Figure 9: Plots of (αhν) squared versus photon energy, hν to determine the band gap energy of nanostructured ZnO thin films deposited at different times. The band gap energies, Eg of each of the samples is indicated in the plot.

Near the band edge, the absorption coefficient is exponentially dependent on the photon energy and this relationship is given by the Urbach's empirical formula given in equation (17) [51].

$$\alpha = \alpha_0 \exp \frac{h\nu}{E_u} \qquad (17)$$

Where hν is the photon energy in eV, α_0 is a constant and E_u is the Urbach energy which corresponds to the width of the exponential tail. This Urbach tail's energy is obtained as the inverse of the slope of the linear part of the plot of ln α with respect to the photon energy as shown in Figure 10. The Urbach energies of 0.119 eV, 0.153 eV, 0.182 eV and 0.193 eV were obtained for 15, 20, 25 and 30 mins deposition times respectively. This Urbach energy increase is attributed to the increase in the disorderliness of the film [52].

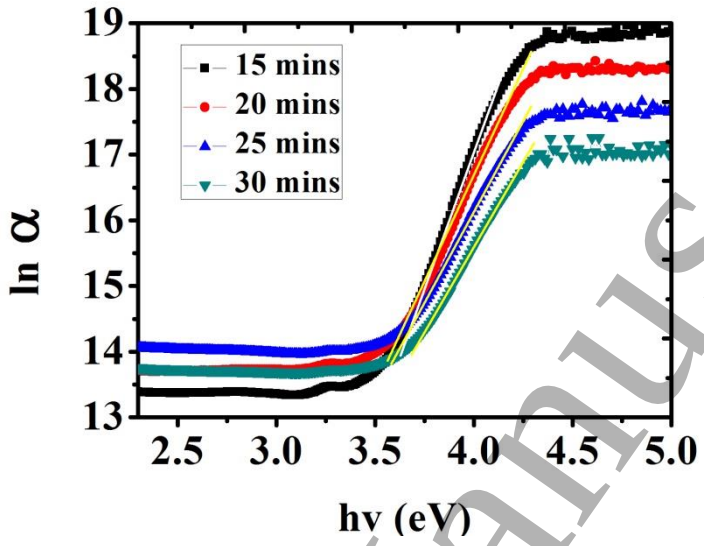

Figure 10: Plot of ln α versus photon energy, hν to obtain the Urbach Energies of nanostructured ZnO thin films at different deposition times.

The refractive index was obtained using equation (18) [50]

$$n = \left(\frac{1+R}{1-R}\right) + \sqrt{\frac{4R}{(1-R)^2} - k^2} \qquad (18)$$

where k, the extinction coefficient.

As expected, an increase in deposition time increased the refractive index of the film as shown in Figure 11. However, at between 25 and 30 mins deposition time, the refractive index maintained an average value of 2.63 eV.

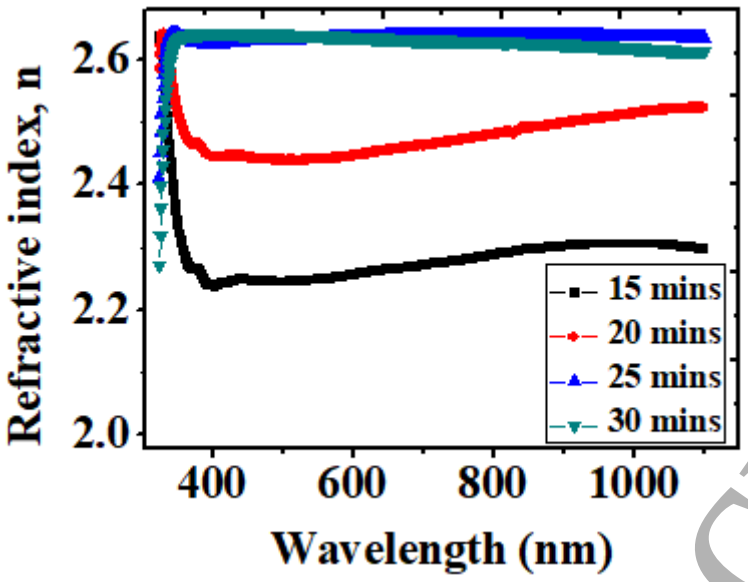

Figure 11: Plot of refractive index as a function of the wavelength of nanostructured ZnO thin films deposited at different times.

The real and imaginary dielectric constants ε_1 and ε_2 of ZnO were obtained using the following relations: $\varepsilon_1 = n^2 - k^2$ and $\varepsilon_2 = 2nk$. Figure 12 (a) and (b) shows the plots of the real and imaginary dielectric constants with respect to wavelength, respectively. ε_1 can be expressed in correlation with the free carrier contribution given by equation (19) [53]

$$\varepsilon_1 = \varepsilon_\infty - \left(\frac{Ne^2}{4\pi^2 c^2 \varepsilon_0 m^*} \right) \lambda^2 \qquad (19)$$

where, $\varepsilon_\infty$is the high frequency dielectric constant, e is the elementary charge, c is the speed of light, ε_0 is the vacuum permittivity, N is the free carrier concentration and m* is the effective mass. Figure 12(c) shows the change in ε_1 with respect to λ^2. The high frequency dielectric constant, ε_∞ was obtained as the vertical intercept of the straight line obtained in the graph.

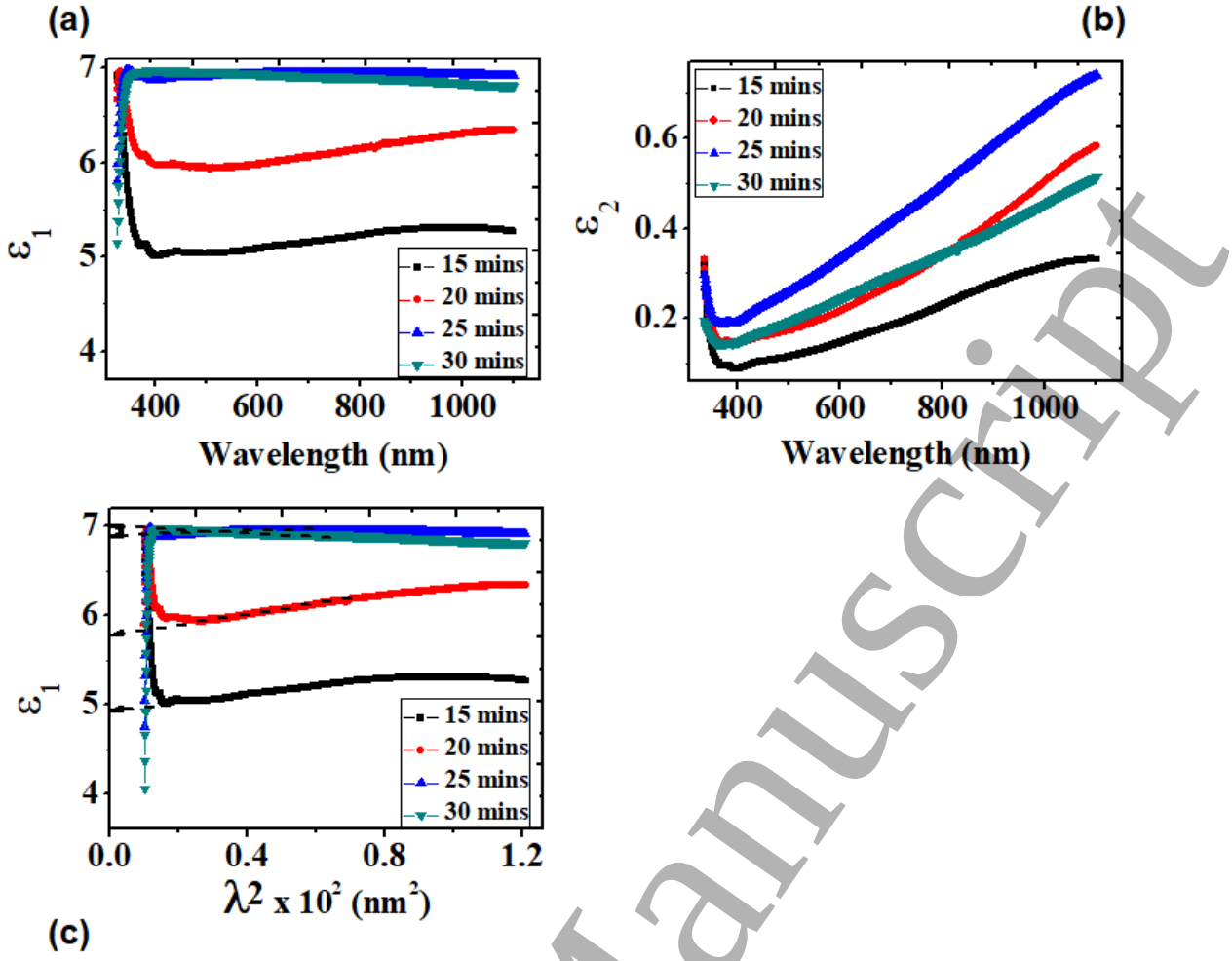

Figure 12: Plots of (a) Real dielectric constant and (b) Imaginary dielectric constant of nanostructured ZnO thin films as a function of wavelength. (c) Real dielectric constant as a function of λ^2

Table 3 shows a summary of the optical parameter obtained in this study. Note that the values of T, A, R, α, n and k are the respective average values in the visible light spectrum (400 to 700 nm).

Table 3: Summary of the optical properties of ZnO obtained at different deposition times.

Deposition time (mins)	T (%)	A (%)	R (%)	E_g (eV)	α (x10^5) (cm^{-1})	E_u (eV)	n	k (x10^{-2})	ε_1	ε_2	ε_∞
15	69	16	15	3.58	6.67	0.119	2.25	2.94	5.07	0.132	4.93
20	61	22	17	3.50	9.23	0.153	2.44	4.05	5.98	0.198	5.78
25	47	33	20	3.46	12.88	0.182	2.63	5.69	6.93	0.299	6.90
30	41	39	20	3.65	9.45	0.193	2.63	4.16	6.95	0.219	7.00

3.5 Raman Spectroscopy

Theoretically, ZnO has a Wurtzite structure, which fits to the space group C_6v^4, with two formula units per primitive cell where the entire atoms occupy the 2b sites of the symmetry C_3v [54–56]. For a perfect ZnO crystal, only the optical phonons at Γ point group of the Brillouin zone are included in the first order Raman scattering [56]. Zone center optical phonons envisages the existence of the resulting modes: Γopt = A_1+2B_1+E_1+2E_2 [57]. The, A_1 and E_1 modes are polar. The polar modes are split further into transverse optical (A_1 TO and E_1TO) and longitudinal optical (A_1TO and E_1TO) components. E_2 mode consists of two modes of low and high of frequency phonons (E_2 low and E_2 high). The E_2 low is related with the vibration of heavy Zn sub lattice, whereas the E_2 high mode is related with vibration of oxygen atoms only.

The phonon frequencies detected in the Raman spectra shown in Figure 13 are: 334 cm^{-1} (E_2(high)-E_2(low)), 435 cm^{-1}(E_2(high)), 578 cm^{-1} (A_1(LO)) and 1092cm^{-1} (2(LO)). This observations confirms the as prepared ZnO nano-petal have a hexagonal Wurtzite structure [58]. These observations are in mutual agreement with XRD analysis that revealed the prepared samples have a Wurtzite crystalline structure. Our Raman analysis has equally shown that there is a decrease in peak intensity with increase in deposition time. This can be attributed to decrease in crystallinity or orderliness of the Wurtzite ZnO structure with increase in deposition times. This observation is in mutual agreement with XRD analysis that has revealed that the intensity of the 002 plane increased as the deposition time increased which indicates crystallite growth was more favoured through 002 plane rather than the normal 001 plane of Wurtzite ZnO. Hence, this led to crystallite distortion as the deposition time was increased. In the same vein, the observation agrees with the calculated urbach energies which increased from 0.119 eV, to 0.193 eV with increase in deposition times from 10 mins to 30 mins respectively. Which further cements that crystallite disorderliness of Wurtzite ZnO increased with increase in deposition times [52].

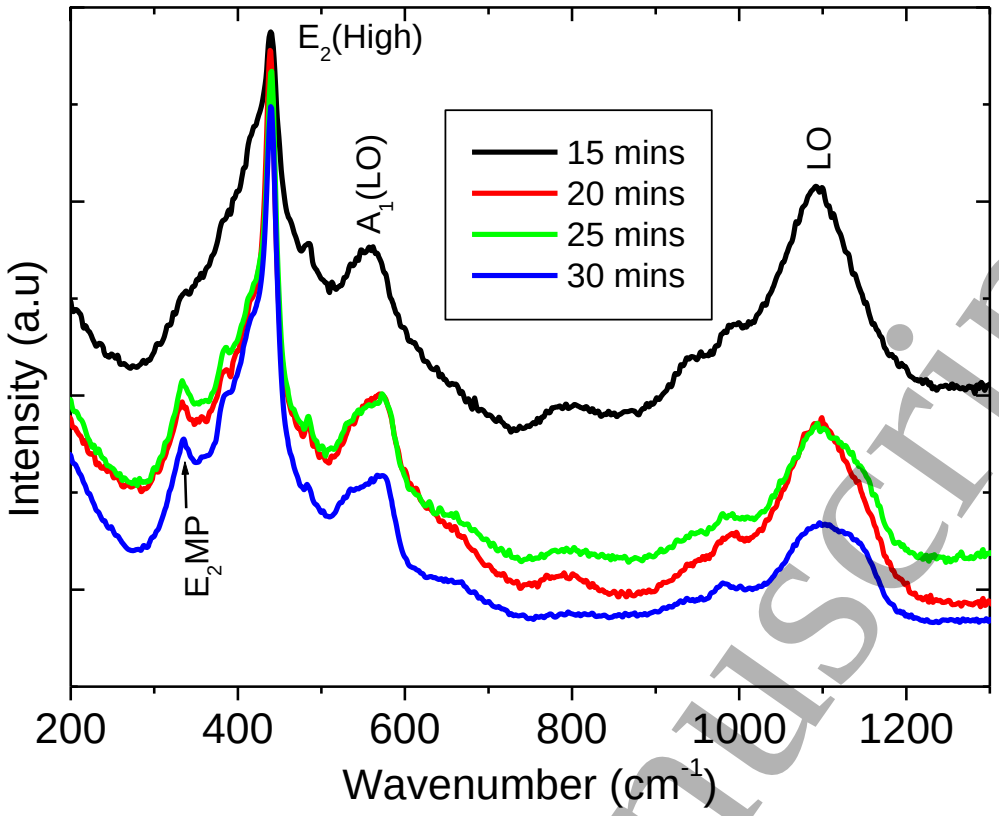

Figure 13: Raman spectra of nanostructured ZnO thin films deposited at 15, 20, 25 and 30 minutes. Peak intensity broadens and increases in height as the deposition time increases from 15 min. to 30 min. Phonon frequencies appear consistently fixed in value in all the samples.

3.6 Electrical Properties

The I-V curves of the ZnO nanostructured thin films are shown in Figure 14(a). The linear I-V curve is an indication that the Al metal contact shows Ohmic behavior with the thin films. Hence, our ZnO films are very conductive. A plot of the film resistivity obtained from the I-V curve and plotted against the film thickness is shown in Panel (b) of Fig. 14. The result shows an increase in resistivity with thickness and hence, with the deposition time. Film thickness can significantly affect the electrical conductivity of ZnO thin films in a variety of ways [60]. In our case, the observed increase of the film resistivity can be attributed to an increase of trapped carriers in the grain boundary since the calculated lattice strain in Table 1 also increased with thickness. Our highly conductive, thinnest ZnO samples are capable of satisfying the thinness requirements of next-generation optoelectronics devices when optimized to form highly homogeneous layer.

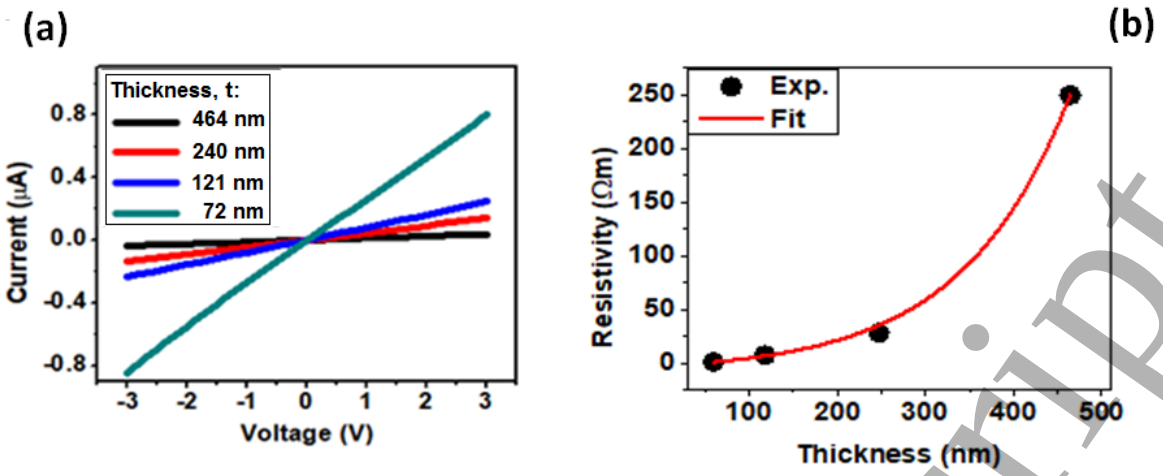

Figure 14: (a) I-V curves of ZnO thin films at four different thicknesses. (b) Film resistivity values obtained from the I-V curves.

4. Conclusion

In this work, ZnO nanoflowers have been synthesized using a modified aqueous chemical growth method on microscope glass slides. SEM analysis has revealed a consistent surface morphology with increase in deposition times. Moreover, this SEM analysis revealed the ideal growth pattern which has been depicted to grown via nucleation and amalgamation of proceeding ZnO nuclei. The theory mechanism behind the portrayed growth pattern has been cross examined using Young-Dupre equations. SEM analysis have shown that the controlled modified chemical bath method adopted in this study can be used as benchmark for preparation of a variety of ZnO nano-structures with a controlled morphology for various applications. XRD analysis has revealed that the synthesized ZnO nano-petals have a Wurtzite structure with peaks at two theta angles of 31.7°, 34.4°, 36.2°, 47.4°, 56.5°and 62.7° respectively belonging to the (100), (002), (101), (102), (110) and (103) planes. Raman analysis has also confirmed the presence of a Wurtzite ZnO structures with Raman vibration frequencies and symmetries at 334 cm^{-1} (E2(high)-E2(low)), 435 cm^{-1}(E2(high)), 578 cm^{-1} (A1(LO)) and 1092cm^{-1} (2(LO)). I-V measurements have revealed that the prepared ZnO nanostructural thin films are highly conductive. I-V analysis has also revealed that the resistivity increased with increase in deposition which has been attributed to increased thin film thickness with deposition times which in turn reduces electron mobility.

Different characterisation techniques were used to obtain the morphology, structure, optical and electrical properties of the samples obtained at different deposition times. An increase in deposition time showed an improvement in the overall structure, crystallinity of ZnO nanopetals. Hence, these parameters can be tuned by changing the deposition time

using this modified aqueous chemical growth method for their applications in numerous fields.

Acknowledgements

We graciously acknowledge the grant for this project by TETFUND under contract number *TETF/DESS/UNN/NSUKKA/STI/VOL.I/B4.33.* We thank the US Army Research Laboratory–Broad Agency Announcement (BAA) for the financial support given to this research (under Contract number W911NF-12-1-0588). The results were also partially developed within the CENTEM project, reg. no. CZ.1.05/2.1.00/03.0088 co-funded by the ERDF within the OP RDI programme, and in the follow-up sustainability stage, supported through CENTEM+ (LO1402) by financial means from the Czech Ministry of Education, Youth and Sports under the National Sustainability Programme. Also we thank Engr. Emeka Okwuosa for generous sponsorship of April 2014, July 2016 and July 2018 conference/workshops on applications of nanotechnology to energy, health &. Environment conference.

References

[1] Y. Zhang, T.R. Nayak, H. Hong, W. Cai, Biomedical applications of zinc oxide nanomaterials, Curr. Mol. Med. 13 (2013) 1633–1645.

[2] S.A. Akhoon, S. Rubab, M.A. Shah, A benign hydrothermal synthesis of nanopencils-like zinc oxide nanoflowers, Int. Nano Lett. 5 (2015) 9–13.

[3] Z.L. Wang, Zinc oxide nanostructures: growth, properties and applications, J. Phys. Condens. Matter. 16 (2004) R829.

[4] F.I. Ezema, U.O.A. Nwankwo, Effect of annealing temperature on the structural and optical properties of zinc oxide (ZnO) nanocrystals prepared by sol gel, Dig. J. Nanomater. Biostructures. 5 (2010) 981–988.

[5] J. Liu, X. Huang, Y. Li, J. Duan, H. Ai, Large-scale synthesis of flower-like ZnO structures by a surfactant-free and low-temperature process, Mater. Chem. Phys. 98 (2006) 523–527.

[6] S.J. Pearton, B.S. Kang, L.C. Tien, D.P. Norton, Y.W. Heo, F. Ren, ZnO-based nanowires, Nano. 2 (2007) 201–211.

[7] Y.W. Chen, Y.C. Liu, S.X. Lu, C.S. Xu, C.L. Shao, C. Wang, J.Y. Zhang, Y.M. Lu, D.Z. Shen, X.W. Fan, Optical properties of ZnO and ZnO: In nanorods assembled by sol-gel method, J. Chem. Phys. 123 (2005) 134701.

[8] C. Li, G. Hong, P. Wang, D. Yu, L. Qi, Wet chemical approaches to patterned arrays of well-aligned ZnO nanopillars assisted by monolayer colloidal crystals, Chem. Mater. 21 (2009) 891–897.

[9] W.L. Hughes, Z.L. Wang, Controlled synthesis and manipulation of ZnO nanorings and nanobows, Appl. Phys. Lett. 86 (2005) 043106.

[10] S. Ameen, M.S. Akhtar, H.S. Shin, Growth and characterization of nanospikes decorated ZnO sheets and their solar cell application, Chem. Eng. J. 195 (2012) 307–313.

[11] M. Chen, Z. Wang, D. Han, F. Gu, G. Guo, Porous ZnO polygonal nanoflakes: synthesis, use in high-sensitivity NO2 gas sensor, and proposed mechanism of gas sensing, J. Phys. Chem. C. 115 (2011) 12763–12773.

[12] R. Wahab, S.G. Ansari, Y.S. Kim, H.K. Seo, G.S. Kim, G. Khang, H.-S. Shin, Low temperature solution synthesis and characterization of ZnO nano-flowers, Mater. Res. Bull. 42 (2007) 1640–1648.

[13] R.C. Wang, C.P. Liu, J.-L. Huang, S.-J. Chen, Y.-K. Tseng, S.-C. Kung, ZnO nanopencils: Efficient field emitters, Appl. Phys. Lett. 87 (2005) 013110.

[14] G.S. Wu, T. Xie, X.Y. Yuan, Y. Li, L. Yang, Y.H. Xiao, L.D. Zhang, Controlled synthesis of ZnO nanowires or nanotubes via sol–gel template process, Solid State Commun. 134 (2005) 485–489.

[15] J.-J. Wu, S.-C. Liu, others, Low-temperature growth of well-aligned ZnO nanorods by chemical vapor deposition, Adv. Mater. 14 (2002) 215.

[16] H.-W. Suh, G.-Y. Kim, Y.-S. Jung, W.-K. Choi, D. Byun, Growth and properties of ZnO nanoblade and nanoflower prepared by ultrasonic pyrolysis, J. Appl. Phys. 97 (2005) 044305.

[17] H.I. Abdulgafour, Z. Hassan, N. Al-Hardan, F.K. Yam, Growth of zinc oxide nanoflowers by thermal evaporation method, Phys. B Condens. Matter. 405 (2010) 2570–2572.

[18] J. Qiu, X. Li, W. He, S.-J. Park, H.-K. Kim, Y.-H. Hwang, J.-H. Lee, Y.-D. Kim, The growth mechanism and optical properties of ultralong ZnO nanorod arrays with a high aspect ratio by a preheating hydrothermal method, Nanotechnology. 20 (2009) 155603.

[19] J. Zhang, W. Wang, P. Zhu, J. Chen, Z. Zhang, Z. Wu, Synthesis of small diameter ZnO nanorods via refluxing route in alcohol–water mixing solution containing zinc salt and urea, Mater. Lett. 61 (2007) 592–594.

[20] R.C. Pawar, J.S. Shaikh, A.A. Babar, P.M. Dhere, P.S. Patil, Aqueous chemical growth of ZnO disks, rods, spindles and flowers: pH dependency and photoelectrochemical properties, Sol. Energy. 85 (2011) 1119–1127.

[21] M. Law, L.E. Greene, J.C. Johnson, R. Saykally, P. Yang, Nanowire dye-sensitized solar cells, Nat. Mater. 4 (2005) 455–459.

[22] Q. Ahsanulhag, A. Umar, Y. B. Hahn, Growth of aligned ZnO nanorods and nanopencils on ZnO/Si in aqueous solution: growth mechanism and structural and optical properties.Nanotechnology 18 (2007) 115603

[23] S.L. Mammah, F.E. Opara, F.B. Sigalo, S.C. Ezugwu, F.I. Ezema, Effect of concentration on the optical and solid state properties of ZnO thin films deposited by Aqueous Chemical Growth (ACG) method, J. Mod. Phys. 3 (2012) 1516.

[24] D. Vernardou, G. Kenanakis, S. Couris, E. Koudoumas, E. Kymakis, N. Katsarakis, pH effect on the morphology of ZnO nanostructures grown with aqueous chemical growth, Thin Solid Films. 515 (2007) 8764–8767.

[25] K.-S. Kim, H.W. Kim, Synthesis of ZnO nanorod on bare Si substrate using metal organic chemical vapor deposition, Phys. B Condens. Matter. 328 (2003) 368–371.

[26] X. Gao, X. Li, W. Yu, Synthesis and characterization of flowerlike ZnO nanostructures via an ethylenediamine-meditated solution route, J. Solid State Chem. 178 (2005) 1139–1144.

[27] J. Duan, X. Huang, E. Wang, PEG-assisted synthesis of ZnO nanotubes, Mater. Lett. 60 (2006) 1918–1921.

[28] K. Govender, D.S. Boyle, P.B. Kenway, P. O'Brien, Understanding the factors that govern the deposition and morphology of thin films of ZnO from aqueous solution, J. Mater. Chem. 14 (2004) 2575–2591.

[29] P. Sangpour, M. Roozbehi, O. Akhavan, A.Z. Moshfegh, ZnO nanowires from nanopillars: Influence of growth time, Curr. Nanosci. 5 (2009) 479–484.

[30] H. Zhu, H. Jia, D. Liu, Y. Feng, L. Zhang, B. Lai, T. He, Y. Ma, Y. Wang, J. Yin, Study of thermal stability of ZnO: B films grown by LPCVD technique, Appl. Surf. Sci. 258 (2012) 6018–6023.

[31] S.C. Ezugwu, F.I. Ezema, P.U. Asogwa, D.D.O. Eya, The effect of deposition time on the structural and optical properties of ZnO thin films by aqueous chemical growth technique, Dig. J. Nanomater. Biostructures DJNB. 6 (2011).

[32] Z. Li, K. Zhu, Q. Zhao, A. Meng, The enhanced SERS effect of Ag/ZnO nanoparticles through surface hydrophobic modification, Appl. Surf. Sci. 377 (2016) 23–29.

[33] M. Volmer and A. Weber, Z Phys. Chem. 199 (1926) 277.

[34] L.E. Murr, Interfacial phenomena in metals and alloys, Reading, MA: Addison-Wesley, 1975.

[35] C.H.P. Lupis, Chemical thermodynamics of materials. 1983, New York, Elsevier Science.

[36] L.-Y. Lin, H.-J. Kim, D.-E. Kim, Wetting characteristics of ZnO smooth film and nanowire structure with and without OTS coating, Appl. Surf. Sci. 254 (2008) 7370–7376.

[37] M. Shaban, M. Zayed, H. Hamdy, Nanostructured ZnO thin films for self-cleaning applications, RSC Adv. 7 (2017) 617–631.

[38] J. Tam, G. Palumbo, U. Erb, Recent advances in superhydrophobic electrodeposits, Materials. 9 (2016) 151.

[39] O. Akhavan, M. Mehrabian, K. Mirabbaszadeh, R. Azimirad, Hydrothermal synthesis of ZnO nanorod arrays for photocatalytic inactivation of bacteria, J. Phys. Appl. Phys. 42 (2009) 225305.

[40] P.S. Kumar, J. Sundaramurthy, D. Mangalaraj, D. Nataraj, D. Rajarathnam, M.P. Srinivasan, Enhanced super-hydrophobic and switching behavior of ZnO nanostructured surfaces prepared by simple solution–immersion successive ionic layer adsorption and reaction process, J. Colloid Interface Sci. 363 (2011) 51–58.

[41] Z. Guo, X. Chen, J. Li, J.-H. Liu, X.-J. Huang, ZnO/CuO hetero-hierarchical nanotrees array: hydrothermal preparation and self-cleaning properties, Langmuir. 27 (2011) 6193–6200.

[42] E. Muchuweni, T.S. Sathiaraj, H. Nyakotyo, Synthesis and characterization of zinc oxide thin films for optoelectronic applications, Heliyon. 3 (2017) e00285.

[43] V.D. Mote, Y. Purushotham, B.N. Dole, Williamson-Hall analysis in estimation of lattice strain in nanometer-sized ZnO particles, J. Theor. Appl. Phys. 6 (2012) 6.

[44] M. Kashif, U. Hashim, M.E. Ali, S.M. Usman Ali, M. Rusop, Z.H. Ibupoto, M. Willander, Effect of different seed solutions on the morphology and electrooptical properties of ZnO nanorods, J. Nanomater. 2012 (2012) 106.

[45] K.L. Foo, U. Hashim, K. Muhammad, C.H. Voon, Sol–gel synthesized zinc oxide nanorods and their structural and optical investigation for optoelectronic application, Nanoscale Res. Lett. 9 (2014) 429.

[46] M.N.H. Mia, M.F. Pervez, M.K. Hossain, M.R. Rahman, M.J. Uddin, M.A. Al Mashud, H.K. Ghosh, M. Hoq, Influence of Mg content on tailoring optical bandgap of Mg-doped ZnO thin film prepared by sol-gel method, Results Phys. 7 (2017) 2683–2691.

[47] S. Aksoy, Y. Caglar, S. Ilican, M. Caglar, Effect of deposition temperature on the crystalline structure and surface morphology of ZnO films deposited on p-Si, Adv. Control Chem. Eng. Civ. Eng. Mech. Eng. ISBN. (2010) 978–960.

[48] U. Seetawan, S. Jugsujinda, T. Seetawan, A. Ratchasin, C. Euvananont, C. Junin, C. Thanachayanont, P. Chainaronk, Effect of calcinations temperature on crystallography and nanoparticles in ZnO disk, Mater. Sci. Appl. 2 (2011) 1302.

[49] S.A. Aly, N.Z. El Sayed, M.A. Kaid, Effect of annealing on the optical properties of thermally evaporated ZnO films, Vacuum. 61 (2001) 1–7.

[50] M. Yıldırım, A. Aljabour, A. Sarılmaz, F. Ozel, Investigation of optical framework of chalcostibite nanocrystal thin films: An insight into refractive index dispersion, optical band gap and single-oscillator parameters, J. Alloys Compd. (2017).

[51] F. Urbach, The long-wavelength edge of photographic sensitivity and of the electronic absorption of solids, Phys. Rev. 92 (1953) 1324.

[52] F. Yakuphanoglu, S. Ilican, M. Caglar, Y. Caglar, The determination of the optical band and optical constants of non-crystalline and crystalline ZnO thin films deposited by spray pyrolysis, J. Optoelectron. Adv. Mater. 9 (2007) 2180.

[53] E.D. Palik, Handbook of optical constants of solids, Academic press, 1998.

[54] A. Bagabas, A. Alshammari, M.F. Aboud, H. Kosslick, Room-temperature synthesis of zinc oxide nanoparticles in different media and their application in cyanide photodegradation, Nanoscale Res. Lett. 8 (2013) 516.

[55] P.K. Giri, S. Bhattacharyya, D.K. Singh, R. Kesavamoorthy, B.K. Panigrahi, K.G.M. Nair, Correlation between microstructure and optical properties of ZnO nanoparticles synthesized by ball milling, J. Appl. Phys. 102 (2007) 093515.

[56] V.A. Fonoberov, A.A. Balandin, ZnO quantum dots: physical properties and optoelectronic applications, J. Nanoelectron. Optoelectron. 1 (2006) 19–38.

[57] A.B. Lavand, Y.S. Malghe, Visible light photocatalytic degradation of 4-chlorophenol using C/ZnO/CdS nanocomposite, J. Saudi Chem. Soc. 19 (2015) 471–478.

[58] M. Schumm, ZnO-based semiconductors studied by Raman spectroscopy: semimagnetic alloying, doping, and nanostructures, JuliusMaximilians-Universität Würzburg, 2008.

[59] C. Soci, A. Zhang, B. Xiang, S.A. Dayeh, D.P.R. Aplin, J. Park, X.Y. Bao, Y.-H. Lo, D. Wang, ZnO nanowire UV photodetectors with high internal gain, Nano Lett. 7 (2007) 1003–1009.

[60] S. Mridha, D. Basak, Effect of thickness on the structural, electrical and optical properties of ZnO films. Material Research Bulletin 42 (2007) 875